ORIGINAL ARTICLE

AASLD
AMERICAN ASSOCIATION FOR
THE STUDY OF LIVER DISEASES

OPEN

Hepatic IL22RA1 deficiency promotes hepatic steatosis by modulating oxysterol in the liver

Yeping Huang[1] | Fan Yu[1] | Yue Ding[2] | Hong Zhang[1] | Xinyue Li[1] |
Xiao Wang[1] | Xiaoshan Wu[3] | Jie Xu[1] | Liang Wang[4] | Chenxu Tian[4] |
Min Jiang[2] | Rong Zhang[1] | Chenyan Yan[5,6] | Yingxiang Song[5,6] |
Haijun Huang[7] | Guangzhong Xu[4] | Qiurong Ding[3] | Xiao Ye[5,6] | Yan Lu[8] |
Cheng Hu[1,9]

[1]Shanghai Diabetes Institute, Shanghai Key Laboratory of Diabetes Mellitus, Shanghai Clinical Centre for Diabetes, Shanghai Sixth People's Hospital Affiliated to Shanghai Jiao Tong University School of Medicine, Shanghai, China

[2]School of Pharmacy, Shanghai University of Traditional Chinese Medicine, Shanghai, China

[3]CAS Key Laboratory of Nutrition, Metabolism and Food Safety, Shanghai Institute of Nutrition and Health, University of Chinese Academy of Sciences, Chinese Academy of Sciences, Shanghai, China

[4]Surgery Centre of Diabetes Mellitus, Capital Medical University Affiliated Beijing Shijitan Hospital, Beijing, China

[5]Department of Endocrinology, Center for General Practice Medicine, Zhejiang Provincial People's Hospital, Affiliated People's Hospital, Hangzhou Medical College. Hangzhou, Zhejiang, China

[6]Key Laboratory for Diagnosis and Treatment of Endocrine Gland Diseases of Zhejiang Province, Hangzhou, Zhejiang, China

[7]Department of Infectious Diseases, Center for General Practice Medicine, Zhejiang Provincial People's Hospital, Affiliated People's Hospital, Hangzhou Medical College, Hangzhou, Zhejiang, China

[8]Institute of Metabolism and Regenerative Medicine, Shanghai Jiao Tong University Affiliated Sixth People's Hospital, Shanghai, China

[9]Institute for Metabolic Disease, Fengxian Central Hospital Affiliated to Southern Medical University, Shanghai, China

Correspondence
Cheng Hu, Shanghai Diabetes Institute, Shanghai Key Laboratory of Diabetes Mellitus, Shanghai Clinical Centre for Diabetes, Shanghai Sixth People's Hospital Affiliated to Shanghai Jiao Tong University School of Medicine, Shanghai, China, 600 Yishan Road, Xuhui District, Shanghai 200233, China.
Email: alfredhc@sjtu.edu.cn

Yan Lu, Institute of Metabolism and Regenerative Medicine, Shanghai Jiao Tong University Affiliated Sixth People's Hospital, Shanghai, China, 600 Yishan Road, Xuhui District, Shanghai, 200233, China.
Email: luyan5011@shsmu.edu.cn

Abstract

Background and Aims: An imbalance in lipid metabolism is the main cause of NAFLD. While the pathogenesis of lipid accumulation mediated by extrahepatic regulators has been extensively studied, the intrahepatic regulators modulating lipid homeostasis remain unclear. Previous studies have shown that systemic administration of IL-22 protects against NAFLD; however, the role of IL-22/IL22RA1 signaling in modulating hepatic lipid metabolism remains uncertain.

Approach and Results: This study shows that hepatic IL22RA1 is vital in

Abbreviations: AAV, adeno-associated virus; ATF3, activating transcription factor 3; 3β HCA, 3 beta-hydroxy-5-cholestenoic acid; CD, chow diet; CYP7A1, cholesterol 7 alpha-hydroxylase; CYP27A1, sterol 27-hydroxylase; CYP7B1, oxysterol 7 alpha-hydroxylase; CYP8B1, sterol-12 alpha-hydroxylase; DNL, de novo lipogenesis; FASN, fatty acid synthase; GFP, green fluorescent protein; H&E, hematoxylin and eosin; HFD, high-fat diet; HFHC, high fructose high cholesterol; HKO, hepatocyte-specific knockout; HLOs, human liver organoids; IL22RA1, IL-22 receptor alpha 1; LXR-alpha, liver X receptor alpha; MPHs, mouse primary hepatocytes; OA, oleic acid; PA, palmitic acid; RNA-seq, RNA-sequencing; SREBF1, sterol regulatory element binding transcription factor 1; STAT3, signal transducer and activator of transcription 3; TG, triglyceride.

Yeping Huang, Fan Yu, Yue Ding, and Hong Zhang contributed equally to this work.

Supplemental Digital Content is available for this article. Direct URL citations are provided in the HTML and PDF versions of this article on the journal's website, www.hepjournal.com.

- -

Xiao Ye, Department of Endocrinology, Center for General Practice Medicine, Zhejiang Provincial People's Hospital, Affiliated People's Hospital, Hangzhou Medical College. Hangzhou, Zhejiang, China.
Email: semper_fi@foxmail.com

hepatic lipid regulation. IL22RA1 is downregulated in palmitic acid-treated mouse primary hepatocytes, as well as in the livers of NAFLD model mice and patients. Hepatocyte-specific *Il22ra1* knockout mice display diet-induced hepatic steatosis, insulin resistance, impaired glucose tolerance, increased inflammation, and fibrosis compared with flox/flox mice. This is attributed to increased lipogenesis mediated by the accumulation of hepatic oxysterols, particularly 3 beta-hydroxy-5-cholestenoic acid (3β HCA). Mechanistically, hepatic IL22RA1 deficiency facilitates 3β HCA deposition through the activating transcription factor 3/oxysterol 7 alpha-hydroxylase axis. Notably, 3β HCA facilitates lipogenesis in mouse primary hepatocytes and human liver organoids by activating liver X receptor-alpha signaling, but IL-22 treatment attenuates this effect. Additionally, restoring oxysterol 7 alpha-hydroxylase or silencing hepatic activating transcription factor 3 reduces both hepatic 3β HCA and lipid contents in hepatocyte-specific *Il22ra1* knockout mice.

Conclusions: These findings indicate that IL22RA1 plays a crucial role in maintaining hepatic lipid homeostasis in an activating transcription factor 3/oxysterol 7 alpha-hydroxylase-dependent manner and establish a link between 3β HCA and hepatic lipid homeostasis.

INTRODUCTION

Increased obesity drives global NAFLD prevalence.[1] NAFLD comprises 2 stages: NAFLD characterized by excessive lipid accumulation and NASH indicating disease progression.[1] Regulating hepatic lipids involves intricate processes like fatty acid uptake, de novo lipogenesis (DNL), and lipid oxidation.[2] DNL, a tightly controlled process converting carbohydrates into fatty acids, relies on insulin signaling and key transcription factors like sterol regulatory element binding protein 1c and Liver X receptors (LXRs).[3] Sterol regulatory element binding protein 1c activates enzymes such as fatty acid synthase (*Fasn*) and stearoyl-CoA desaturase 1 (*Scd1*) in DNL.[3] In conditions like obesity, uncontrollable DNL leads to excessive triglyceride accumulation.[3] Consequently, modulating hepatic lipogenesis shows potential for NAFLD treatment.[4]

IL-22, a secretory protein produced by innate lymphoid cells,[5] offers tissue repair benefits[5] and protects against NAFLD by preventing hepatocyte apoptosis, modulating lipid metabolism, and enhancing insulin sensitivity.[6] These effects involve signal transducer and activator of transcription 3 (STAT3) and protein kinase B pathways.[5,7,8] IL-22 signals through binding to a receptor complex comprising IL-22 receptor alpha 1 (IL22RA1) subunit, and an IL-10 receptor beta subunit.[5] IL22RA1, the functional receptor of IL-22, is exclusively expressed in metabolic tissues like the liver, pancreas, and intestine.[5] IL22RA1 also pairs with IL20R2 to form the receptor for IL-20 and IL-24.[5] While only IL-22 activates STAT3 in hepatocytes, IL-20 and IL-24 have minimal impact on metabolic disorders.[7] Targeting the IL-22/IL22RA1 pathway shows promise for NAFLD treatment due to its tissue-protective and metabolic effects, without affecting the immune system.[9] Understanding the exact function of IL22RA1 in hepatocytes and its role in NAFLD requires further exploration.

Oxysterols are crucial for metabolic regulation and possess therapeutic potential. They are bioactive lipids produced from cholesterol through specific reactions.[10] These compounds impact immune, inflammatory processes, and metabolic syndrome. An imbalance in oxysterols due to disruptions in cholesterol homeostasis can harm metabolic homeostasis.[10] For instance, systemic administration or hepatic accumulation of 17-hydroxyprogesterone, an intermediate steroid formed during the conversion of cholesterol to cortisol, causes hyperglycemia and insulin resistance in mice.[11] Conversely, elevated 25-hydroxycholesterol levels alleviate hepatic steatosis.[12] Despite their importance in metabolic diseases, the specific connections between endogenous oxysterols and hepatic lipid metabolism are not fully understood.

Here, we investigated the role of IL-22/IL22RA1 in hepatocytes during NAFLD progression using multiple mouse models. We demonstrated that IL22RA1 expression decreased in obesity-related fatty livers both in murine models and humans, as well as in palmitic acid-treated mouse primary hepatocytes (MPHs).

Hepatocyte-specific *Il22ra1*-knockout (HKO) mice exhibited aggravated hepatic steatosis on high-fat diet (HFD) and high fructose high cholesterol (HFHC) diets. Mechanistically, IL22RA1 deficiency in hepatocytes exacerbates hepatic steatosis through 3 beta-hydroxy-5-cholestenoic acid (3β HCA)-mediated lipogenesis, involving activating transcription factor 3 (ATF3)/oxysterol 7 alpha-hydroxylase (CYP7B1) axis. These findings highlight the pro-lipogenic effects of 3β HCA and emphasize the role of hepatocyte IL22RA1 in NAFLD progression.

METHODS

Human liver tissues

Human liver samples (excluding those with steatosis caused by alcohol, hepatitis virus, drug use, or toxins) were obtained from Capital Medical University Affiliated Beijing Shijitan Hospital (Ethics approval number: sjtky11-1x-2022[098]), with written informed consent collected from all individuals. Clinical characteristics are provided in Supplemental Table S1, http://links.lww.com/HEP/I534. The study followed the ethical guidelines outlined in the 1975 Declaration of Helsinki and was approved by the Ethics Committee of Capital Medical University Affiliated Beijing Shijitan Hospital.

Generation of hepatocyte-specific *Il22ra1* knockout mice

HKO mice were generated by introducing loxP sites into *Il22ra1* exon 2 using CRISPR/Cas9 and Cre-loxP technology. Two sgRNAs targeted the exon, enabling loxP insertion through homologous recombination. This involved injecting sgRNAs, oligo donors, and Cas9 mRNA into C57BL/6J zygotes (GemPharmatech, Nanjing, China). A founder mouse was bred with a C57BL/6J mouse to establish *Il22ra1*-flox mice. Crossing these mice with *Alb*-Cre transgenic mice to produce HKO mice, with *Il22ra1*-flox littermates as controls. PCR, DNA sequencing, and qPCR validated exon deletion, with genotyping primers listed in Supplemental Table S2, http://links.lww.com/HEP/I534.

Public RNA-sequencing data and single-nucleus RNA-sequencing data analysis

The single-nucleus RNA-sequencing (RNA-seq) data was retrieved from the GEO database: Hepatocytes demarcated by EphB2 contribute to the progression of NASH (GSE189600).[13] This analysis was performed using 3 normal human livers and 3 NASH human livers. The RNA-seq data was obtained from the GEO database: Transcriptomic profiling across the spectrum of NAFLD (GSE135251).[14] These data comprise 206 snap-frozen biopsy samples from 206 patients diagnosed with NAFLD.

Other methods

The following methods are described in the Supporting Information, including animal experiments, adeno-associated virus (AAV)-mediated and adenovirus-mediated gene manipulation, hepatic and serum biochemical assays, histological analyses, glucose and insulin tolerance tests, luciferase reporter assay, RNA isolation, reverse transcription-qPCR, RNA-seq, western blotting, immunofluorescence staining, primary hepatocyte isolation, cell culture, enzyme-linked immunosorbent assay, bile acid quantification, oxysterol analysis, chromatin immunoprecipitation, Biacore assays, and human liver organoids generation.

Statistical analysis

Statistical analyses were performed using GraphPad Prism software (version 8.2.1; GraphPad Software Inc., La Jolla, CA). Data are presented as mean (SEM). A two-tailed, unpaired Student *t*-test was employed for comparisons between 2 groups, and one-way ANOVA was used for comparisons among 3 groups. Significant differences are indicated as $*p < 0.05$, $**p < 0.01$, $***p < 0.001$.

RESULTS

IL-22 overexpression protects against HFD-induced hepatic steatosis

To assess the impact of AAV-mediated IL-22 overexpression on hepatic steatosis, 7-week-old C57BL/6J mice were fed an HFD for 8 weeks and then administered tail vein injections of AAV-IL-22 or AAV-green fluorescent protein (GFP) (Figure 1A). ELISA validated increased serum IL-22 levels in AAV-IL-22 mice (Figure 1B). While body weights remained similar between groups (Figure 1C), IL-22-overexpressing mice exhibited reduced liver weights (Figure 1D and E), liver-to-body weight ratios (Figure 1F), and milder hepatic steatosis, indicated by lower liver triglyceride (TG) levels (Figure 1G) compared to controls. Oil Red O and hematoxylin and eosin staining of liver sections corroborated decreased lipid accumulation in AAV-IL-22 mice (hematoxylin and eosin [H&E]; Figure 1I). IL-22 overexpression significantly lowered the expression of lipogenic genes, as confirmed using quantitative PCR (qPCR) and western blots (Figure 1J and K). However, the difference in fatty acid–
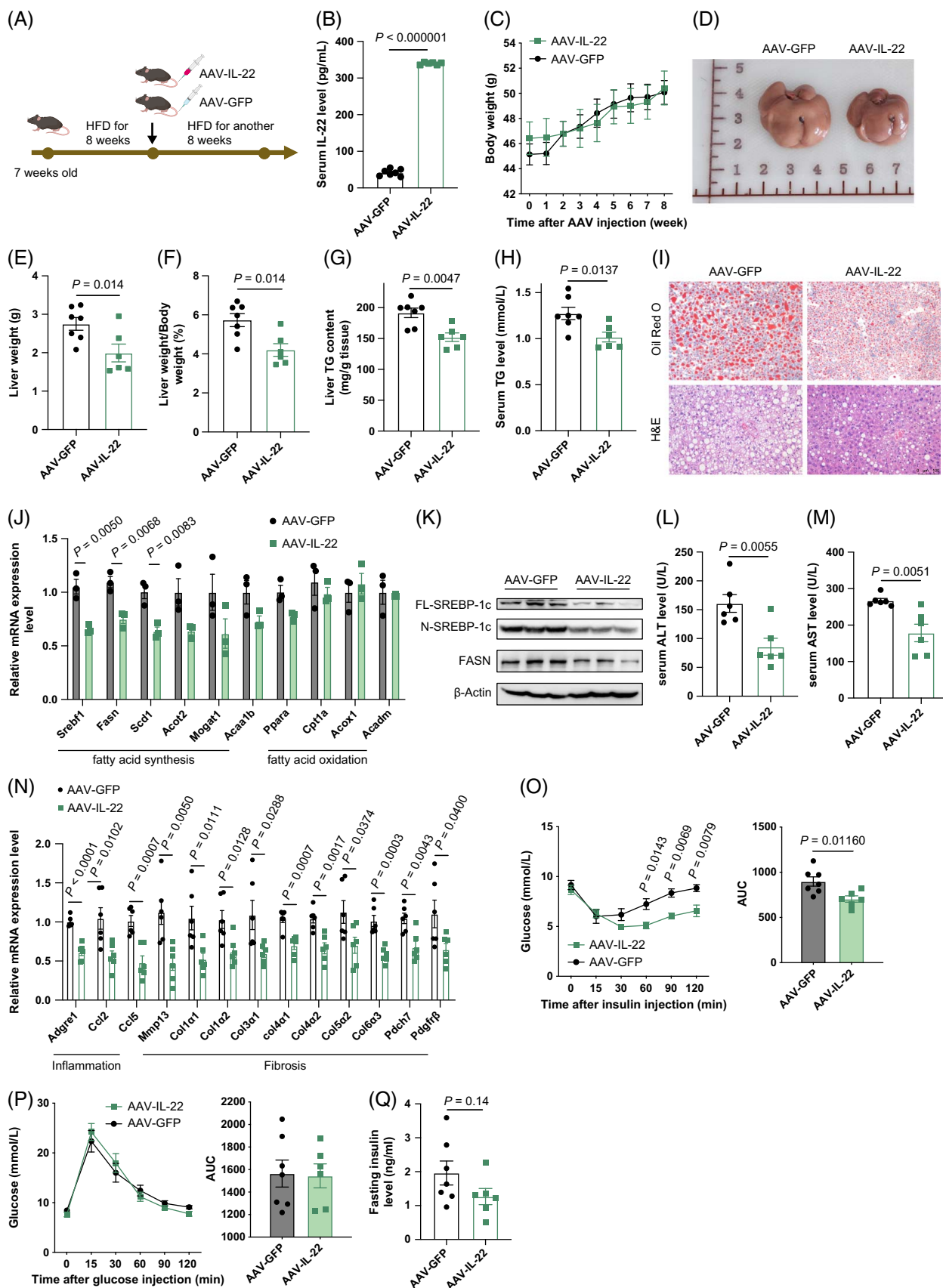
FIGURE 1 IL-22 overexpression protects against HFD-induced hepatic steatosis. Mice were fed a high-fat diet for 8 weeks and then i.v. injected with adeno-associated virus expressing interleukin-22 (AAV-IL-22 or AAV-green fluorescent protein (AAV-GFP). They were subsequently subjected to a high-fat diet for another 8 weeks. (A) Schematic diagram illustrating the study design for AAV-mediated IL-22 overexpression in

oxidation gene expression between these 2 groups was insignificant (Figure 1J). Additionally, liver injury marker, serum ALT (Figure 1L), AST Figure 1M, and TG levels (Figure 1H) were substantially decreased in HFD-fed AAV-IL-22 mice. IL-22 overexpression also correlated with decreased expression of genes involved in inflammation and fibrosis (Figure 1N). I.p. insulin tolerance test indicated enhanced insulin sensitivity in AAV-IL-22 mice compared to controls (Figure 1O), though fasting serum insulin levels and glucose tolerance did not significantly differ between groups (Figure 1Q and P). These data demonstrated that IL-22 alleviated HFD-induced NAFLD progression.

Similarly, under chow diet (CD) conditions, AAV-IL-22 mice exhibited lower hepatic TG than controls (Supplemental Fig. S1E, http://links.lww.com/HEP/I535). Oil Red O and H&E staining of the liver sections confirmed this reduction (Supplemental Fig. S1D, http://links.lww.com/HEP/I535). AAV-IL-22 mice exhibited decreased serum ALT levels and slightly improved insulin sensitivity relative to controls (Supplemental Fig. S1G and J, http://links.lww.com/HEP/I535). However, liver weights (Supplemental Fig. S1B, http://links.lww.com/HEP/I535), liver-to-body weight ratio (Supplemental Fig. S1C, http://links.lww.com/HEP/I535), body weights (Supplemental Fig. S1I, http://links.lww.com/HEP/I535), AST (Supplemental Fig. S1H, http://links.lww.com/HEP/I535), serum TG levels (Supplemental Fig. S1F, http://links.lww.com/HEP/I535), and glucose tolerance were comparable between the 2 groups (Supplemental Fig. S1K, http://links.lww.com/HEP/I535). These findings suggest that IL-22 also reduces hepatic TG content in mice fed a CD that mimics physiological status.

IL22RA1 expression is decreased in fatty liver and PA-treated mouse primary hepatocytes

We explored the endogenous role of IL22RA1 by assessing its expression in 3 NAFLD mouse models. Western blot analysis of the liver samples revealed downregulation of IL22RA1 protein levels in HFD, *db/db*, and *ob/ob* mice compared to normal controls (Figure 2A–C). Experiments using palmitic acid-treated

MPHs also showed a gradual reduction in IL22RA1 expression with increasing palmitic acid concentrations (Figure 2D). Additionally, reduced IL22RA1 protein levels were observed in HFHC diet-induced NASH mice and patients with NAFLD compared to healthy individuals (Figure 2E and F). Single-nucleus RNA-seq revealed enriched *IL22RA1* mRNA expression in hepatocytes compared to nonparenchymal liver cells in human liver samples (Figure 2G),[13] a finding validated through qPCR analysis in mouse hepatocytes (Figure 2H).

Hepatocyte-specific IL22RA1 deficiency exacerbates HFD-induced hepatic steatosis and HFHC-induced NASH

To study the impact of IL22RA1 on liver lipid metabolism, we analyzed mice with HKO (Supplemental Fig. S2A, http://links.lww.com/HEP/I536). qPCR, western blotting, and immunofluorescence staining of liver tissue demonstrated knockout of IL22RA1 in the liver of HKO mice without affecting other tissues (Supplemental Fig. S2B–D, http://links.lww.com/HEP/I536). Primary hepatocytes from HKO mice did not show elevated phosphor (p)-STAT3 levels following IL-22 stimulation, indicating effective IL22RA1 knockout (Supplemental Fig. S2E, http://links.lww.com/HEP/I536). Although liver weights (Supplemental Fig. S2G, http://links.lww.com/HEP/I536), liver-to-body weight ratios (Supplemental Fig. S2H, http://links.lww.com/HEP/I536), serum TG levels (Supplemental Fig. S2M, http://links.lww.com/HEP/I536), and body weights were similar between the flox/flox and HKO littermates fed a CD (Supplemental Fig. S2N, http://links.lww.com/HEP/I536), the HKO mice showed a trend towards more severe hepatic steatosis, as evidenced by slightly higher TG content and lipid accumulation in the liver (Supplemental Fig. S2I and L, http://links.lww.com/HEP/I536). Moreover, HKO mice had higher serum ALT and AST levels (Supplemental Fig. S2J and K, http://links.lww.com/HEP/I536), slightly impaired glucose tolerance (Supplemental Fig. S2O, http://links.lww.com/HEP/I536), and insulin tolerance (Supplemental Fig. S2P, http://links.lww.com/HEP/I536) compared to controls, suggesting that hepatic IL22RA1 deficiency contributes to TG accumulation, even under CD-fed conditions.
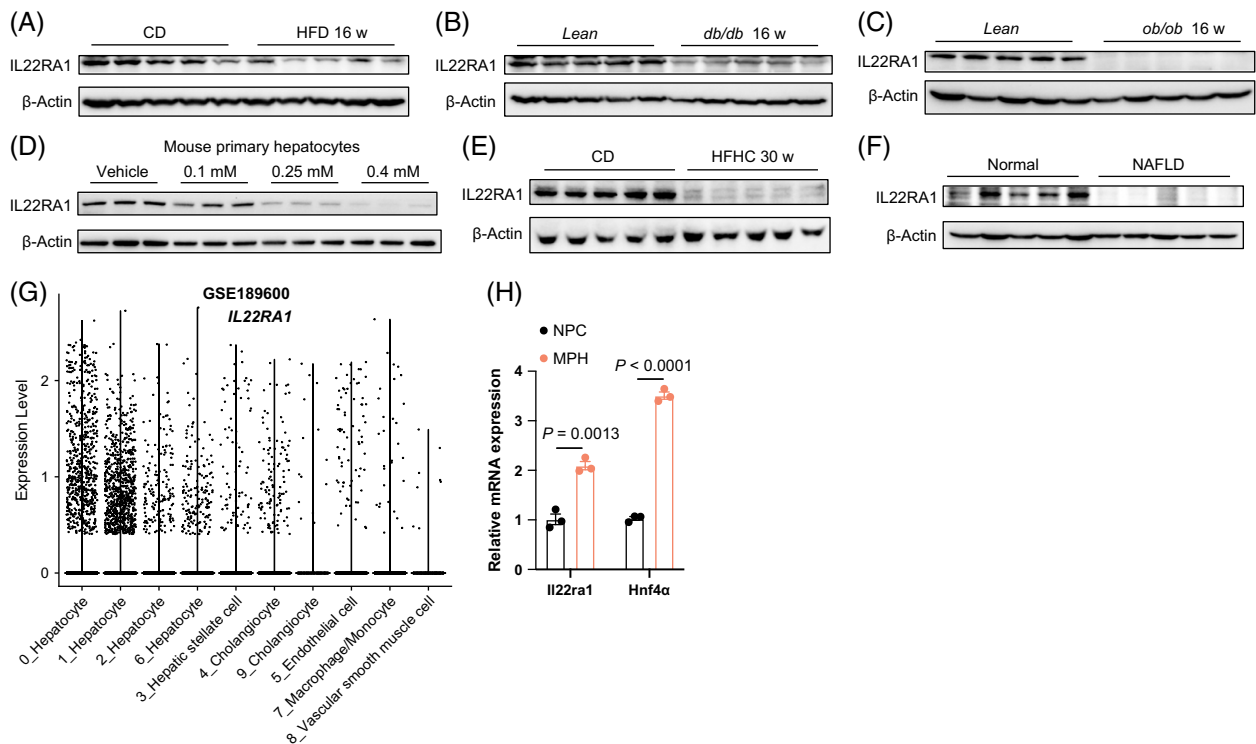
FIGURE 2 IL22RA1 expression is decreased in fatty liver and PA-treated mouse primary hepatocytes. (A–C) Western blot analysis of IL22RA1 expression in the livers from (A) C57BL/6J male mice fed either a chow diet (CD) or an HFD (16 weeks) (n = 5); (B) *lean* and *db/db* mice fed a chow diet for 16 weeks (n = 5); (C) *lean* and *ob/ob* mice fed a chow diet for 16 weeks (n = 5). (D) Western blot analysis of IL22RA1 expression in mouse primary hepatocytes treated with varying concentrations of palmitic acid (0.1 mM, 0.25 mM, 0.4 mM). (E) Western blot analysis of IL22RA1 expression from C57BL/6J male mice fed either a CD or an HFD containing HFHC for 30 weeks (n = 5). (F) Protein levels of IL22RA1 in normal and individuals with NAFLD (n = 5). (G) Single-nucleus RNA sequencing analysis of the distribution of *IL22RA1* gene in human liver based on public single-nucleus RNA sequencing data (GSE189600). (H) mRNA expression levels of *Il22ra1* and *Hnf4α* in NPC and mouse primary hepatocytes. Data are presented as mean ± SEM. For statistical analysis in (H), significance was determined using the Student two-tailed *t*-test. Abbreviations: CD, chow diet; *db/db*, leptin receptor-deficient mice; HFD, high-fat diet; HFHC, high fructose and high cholesterol (also known as GAN diet); MPH, mouse primary hepatocytes; NPC, nonparenchymal cells; *ob/ob*, leptin-deficient mice.

When fed an HFD to induce steatosis, HKO mice showed increased weight gain after 4 weeks of feeding compared to controls. By the seventh week of HFD, body weight became more pronounced, peeking by the eighth week (Supplemental Fig. S3A, http://links.lww.com/HEP/I537). Under HFD conditions, HKO mice exhibited higher liver weights (Figure 3A and B), liver-to-body weight ratio (Figure 3C), and liver TG content than flox/flox mice (Figure 3D). Hepatic TG accumulation in HKO mice was confirmed using Oil Red O staining and H&E staining (Figure 3G). However, the serum TG levels were comparable between the 2 groups (Supplemental Fig. S3B, http://links.lww.com/HEP/I537). The expression of lipogenic genes was significantly elevated in the liver of HKO mice (Figure 3H and I), while fatty acid beta-oxidation gene expression was comparable between the 2 groups (Figure 3H), consistent with minimal changes in metabolic rates (Supplemental Fig. S3C–H, http://links.lww.com/HEP/I537). Corresponding with elevated steatosis, serum ALT and AST levels were significantly increased in HKO mice (Figure 3E and F), indicating enhanced liver damage. Despite elevated hepatic steatosis, significant fibrosis did not occur with an HFD alone.[15] However, HKO mice exhibited increased inflammation and fibrosis gene expression in the liver relative to controls, as identified through RNA-seq and qPCR (Supplemental Fig. S3I and J, http://links.lww.com/HEP/I537). IL22RA1 deficiency exacerbated insulin resistance and glucose intolerance (Supplemental Fig. S3K and L, http://links.lww.com/HEP/I537), as shown by i.p. insulin tolerance test and i.p. glucose tolerance test. Increased insulin resistance led to higher fasting serum insulin levels in HKO mice compared to controls (Supplemental Fig. S3M, http://links.lww.com/HEP/I537). Collectively, these results indicate that IL22RA1 deficiency in hepatocytes exacerbates diet-induced steatosis and disrupts glucose homeostasis.

We further investigated the role of hepatocyte IL22RA1 in HFHC diet-induced NASH. Following HFHC diet feeding, HKO mice exhibited comparable body weights but slightly higher liver weights (Supplemental Fig. S3N and O, http://links.lww.com/HEP/I537), and liver-to-body weight ratio than controls (Figure 3K). HKO mice displayed

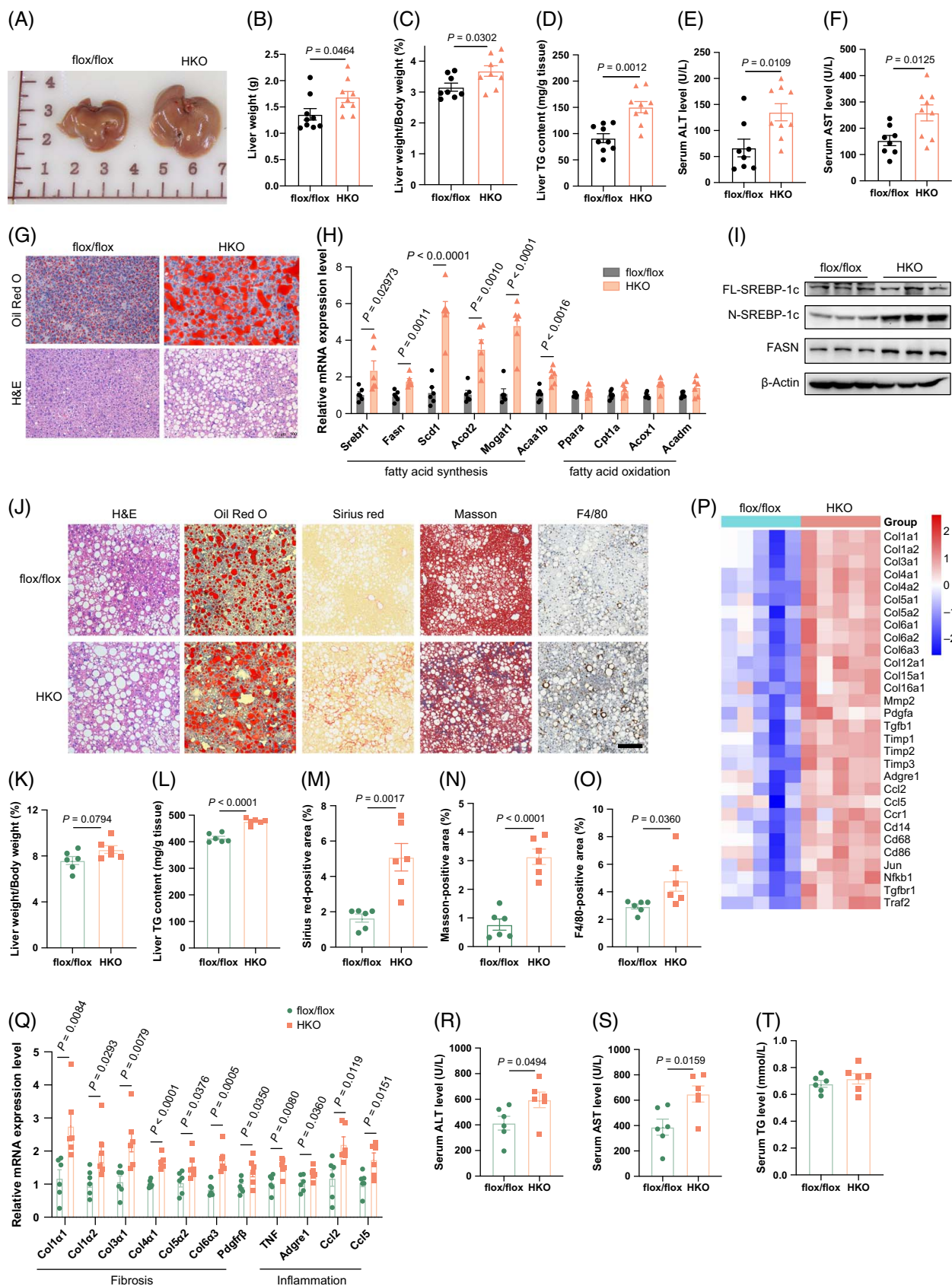**FIGURE 3** Hepatocyte-specific IL22RA1 deficiency exacerbates HFD-induced hepatic steatosis and HFHC-induced NASH. (A-I) Flox/flox and HKO mice were fed a high-fat diet starting at 8 weeks of age for 8 weeks. (A) Representative images of the livers (n = 9). (B, C) Liver weight (B) and liver-to-body weight ratio (C) (n = 8–9). (D) Hepatic TG content. (E, F) Serum ALT (E), and AST levels (F) (n = 8–9).

(G) Representative images of Oil Red O (upper panel) and H&E (lower panel) stained liver sections (n = 9). Scale bar, 100 μm. (H) mRNA levels of genes involved in fatty acid synthesis and oxidation (n = 6). (I) Western blots analysis of lipogenic genes (n = 3). (J–T) Flox/flox and HKO mice were fed an HFHC diet starting at the age of 8 weeks for 28 weeks. (J) H&E, Oil Red O, Sirius red, Masson, and F4/80 staining of liver sections (n = 6). Scale bar, 100 μm. (K) Liver-to-body weight ratio (n = 6). (L) Hepatic TG contents (n = 6). (M–O) Quantification of Sirius red staining (M), Masson staining (N), and F4/80 staining (O) (n = 6). (P) The heatmap displayed genes linked to fibrosis and inflammation in the livers of flox/flox and HKO mice that were fed an HFHC diet, as identified through RNA sequencing. (Q) Relative mRNA levels of genes related to fibrosis and inflammation (n = 6). (R–T) Serum ALT (R), AST (S), and TG (T) levels (n = 6). Data are presented as mean ± SEM. For (B–F), (H), (K–O), and (Q–T), significance was determined using the Student two-tailed t-test. Abbreviations: HFD, high-fat diet; HFHC, high fructose and high cholesterol; HKO, hepatocyte-specific *Il22ra1* knockout; Srebf1, sterol regulatory element binding transcription factor 1; TG, triglyceride.

aggravated liver steatosis, evidenced by H&E staining, Oil Red O staining (Figure 3J), and increased hepatic TG contents (Figure 3L). Mice with IL22RA1-deficient hepatocytes demonstrated elevated collagen deposition, as evidenced by Sirius red staining (Figure 3J), Masson staining (Figure 3J), along with higher mRNA expression levels of fibrogenesis-related genes in the liver compared to flox/flox mice (Figure 3P and Q), indicating escalated liver fibrosis. Inflammatory responses, as revealed by the F4/80 immunohistochemistry of liver section (Figure 3J), and mRNA expression levels of inflammation-related genes in the liver (Figure 3P and Q), were higher in HKO mice than controls. Serum ALT and AST levels were notably elevated in HKO mice compared to flox/flox mice (Figure 3R and S), while serum TG levels remained unaltered (Figure 3T). These findings suggest that the absence of IL22RA1 in hepatocytes contributed to NASH development.

IL-22 overexpression induces while hepatic IL22RA1 deficiency reduces CYP7B1 expression in the liver

Having determined that IL-22 overexpression alleviated steatosis, whereas hepatocyte-specific IL22RA1 deficiency aggravated it, we delved into the molecular mechanism of the IL-22/IL22RA1 signaling in regulating hepatic lipid. To achieve this, we performed RNA-seq using liver tissues from multiple animal models: AAV-IL-22-mice and AAV-GFP mice on CD or HFD, and HFD-fed HKO and flox/flox mice. We conducted GO analysis on differentially expressed genes between the following pairs: CD-fed AAV-IL-22 and AAV-GFP; HFD-fed AAV-IL-22 and AAV-GFP; and HFD-fed HKO and flox/flox mice. In the three pairs, the lipid metabolic process emerged as the most enriched biological process (Figure 4A–C). We identified 12, 71, and 77 differentially expressed genes related to lipid metabolic across these pairs. Notably, *Cyp7b1*, which encodes oxysterol 7 alpha-hydroxylase, a key enzyme in the alternate pathway in bile acid synthesis,[16] emerged as a common gene (Figure 4D).

Subsequently, we validated the expression of CYP7B1 in different animal models. In AAV-IL-22 mice on CD or HFD, both protein and mRNA levels of CYP7B1 increased in the liver (Figure 4E–H), aligning with RNA-seq results.

However, genes encoding other bile acid synthesis enzymes like *Cyp8b1* and *Cyp27a1*[16] remained largely unaffected, except for elevated *Cyp7a1* mRNA levels in the HFD-fed mice (Figure 4F). Conversely, hepatic IL22RA1-deficient mice exhibited decreased CYP7B1 expression in both CD-fed and HFD-fed HKO mice compared with flox/flox mice (Figure 4I–L). Expression levels of *Cyp7a1*, *Cyp8b1*, and *Cyp27a1* were minimally changed in flox/flox and HKO mice, except for decreased *Cyp27a1* mRNA levels in CD-fed HKO mice (Figure 4I–L). *Nr1h4* (encoding farnesoid X receptor, FXR) and *Nr0b2* (encoding small heterodimer partner, SHP) levels, key regulators of bile acid synthesis, were unaltered in the liver of IL-22 overexpression and IL22RA1-deficient mice compared to controls (Figure 4E–L). These data imply that CYP7B1 may be a key target gene influencing liver lipid metabolism mediated by IL-22 signaling.

CYP7B1 replenishment reverses HFD-induced hepatic steatosis in HKO mice

Given that hepatic CYP7B1 levels decreased in HKO mice, we investigated whether replenishment of CYP7B1 could alleviate HFD-induced accentuation of hepatic steatosis. We use viral vectors to boost hepatic CYP7B1 expression by transducing mice with AAV8 virus particles carrying GFP or mouse CYP7B1 (Figure 5A). HKO-AAV-NC mice showed reduced CYP7B1 expression compared to flox/flox-AAV-NC mice, while HKO-AAV-*Cyp7b1* mice exhibited CYP7B1 overexpression in the liver (Figure 5B). Under HFD conditions, HKO-AAV-*Cyp7b1* mice showed blunted weight gain, notably differing after 4 weeks of HFD feeding compared with HKO-AAV-NC mice (Figure 5C). The weight difference continued to expand over the 8-week observation period. Gross morphological changes in the liver size and color were evident between the 2 groups (Figure 5D), with HKO-AAV-*Cyp7b1* mice displaying lower liver weights, liver TG content, and liver-to-body weight ratio (Figure 5E–G). Oil Red O and H&E staining of liver sections confirmed diminished lipid droplet formation in HKO-AAV-*Cyp7b1* mice (Figure 5H), owning to suppressed lipogenic genes in the liver of HKO-AAV-*Cyp7b* mice compared to HKO-AAV-NC mice (Figure 5J and K). Furthermore, HKO-AAV-*Cyp7b1*
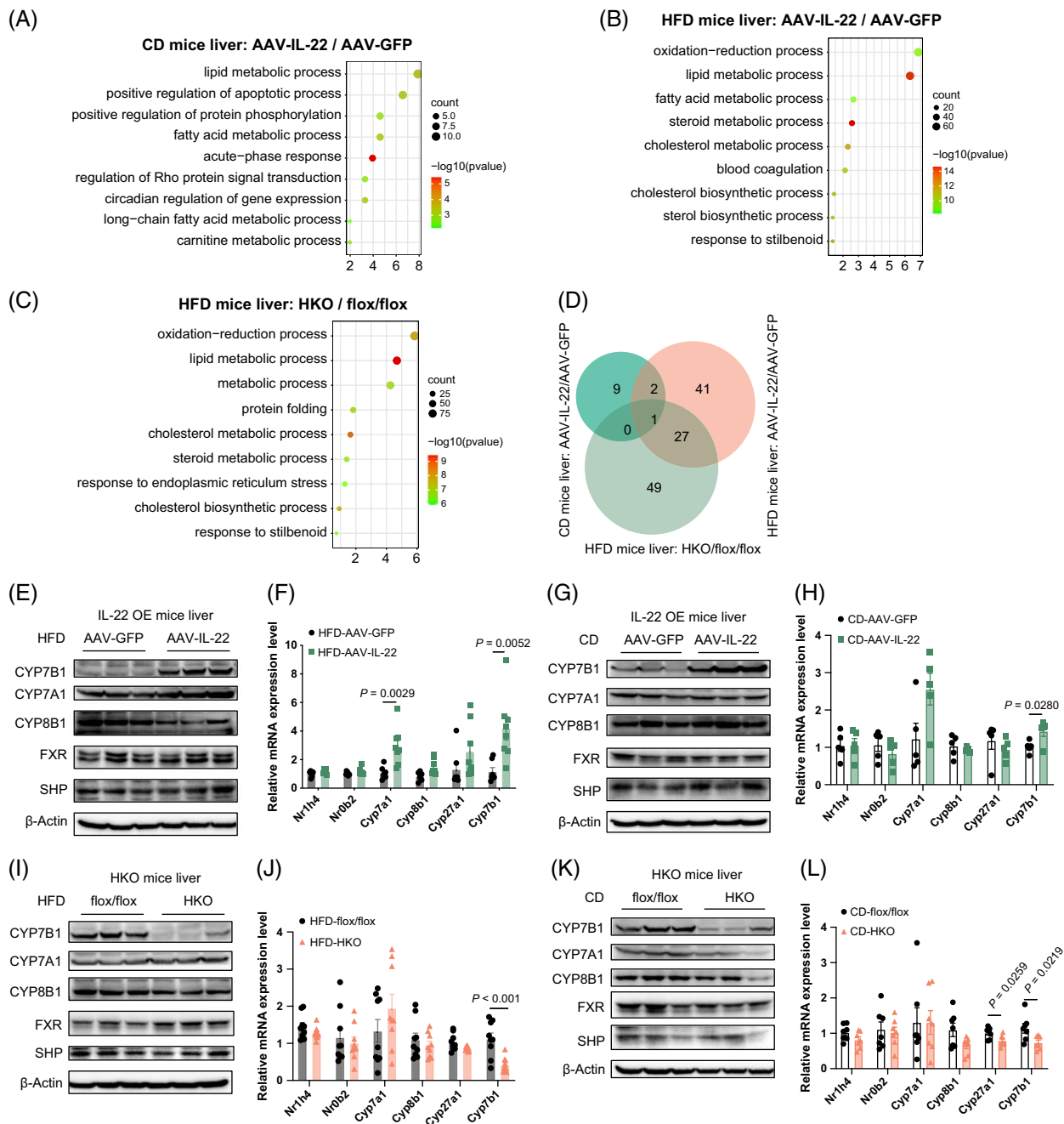
FIGURE 4 IL-22 overexpression induces while IL22RA1 deficiency reduces CYP7B1 expression in the liver. (A) Statistically significant ($p <$ 0.05) differentially regulated biological processes in chow diet (CD)-fed AAV-IL-22 and AAV-GFP mice ($n = 2$). (B) Statistically significant ($p <$ 0.05) differentially regulated biological processes in HFD-fed AAV-IL-22 and AAV-GFP mice ($n = 3$). (C) Hallmark biological processes from enrichment analysis using differentially ($p < 0.05$) expressed genes in HFD-fed flox/flox and HKO mice ($n = 4$–6). (D) Venn diagram displaying overlapping genes in lipid metabolic process from 3 comparative analyses. The protein levels ($n = 3$) (E) and mRNA expression ($n = 7$–8) (F) of the key enzymes and molecular responsible for modulating bile acid synthesis in whole liver lysates from HFD-fed AAV-IL-22 and AAV-GFP mice. The protein levels ($n = 3$) (G) and mRNA expression ($n = 5$) (H) of the key enzymes and molecular responsible for modulating bile acid synthesis in whole liver lysates from CD-fed AAV-GFP and AAV-IL-22 mice. The protein levels ($n = 3$) (I) and mRNA expression ($n = 9$) (J) of the key enzymes and molecular responsible for regulating bile acid synthesis in whole liver lysates from HFD-fed flox/flox and HKO mice. The protein levels ($n = 3$) (K) and mRNA expression ($n = 7$) (L) of the key enzymes and molecular responsible for regulating bile acid synthesis in the livers of CD-fed flox/flox and HKO mice. Data are presented as mean ± SEM. For (F), (H), (J), and (L), significance was determined using the Student two-tailed *t*-test. Abbreviations: AAV, adeno-associated virus; CD, chow diet; CYP7A1, cholesterol 7 alpha-hydroxylase; CYP27A1, sterol 27-hydroxylase; CYP7B1, oxysterol 7 alpha-hydroxylase; CYP8B1, Sterol-12 alpha-hydroxylase; HFD, high-fat diet; HKO, hepatocyte-specific *Il22ra1* knockout.
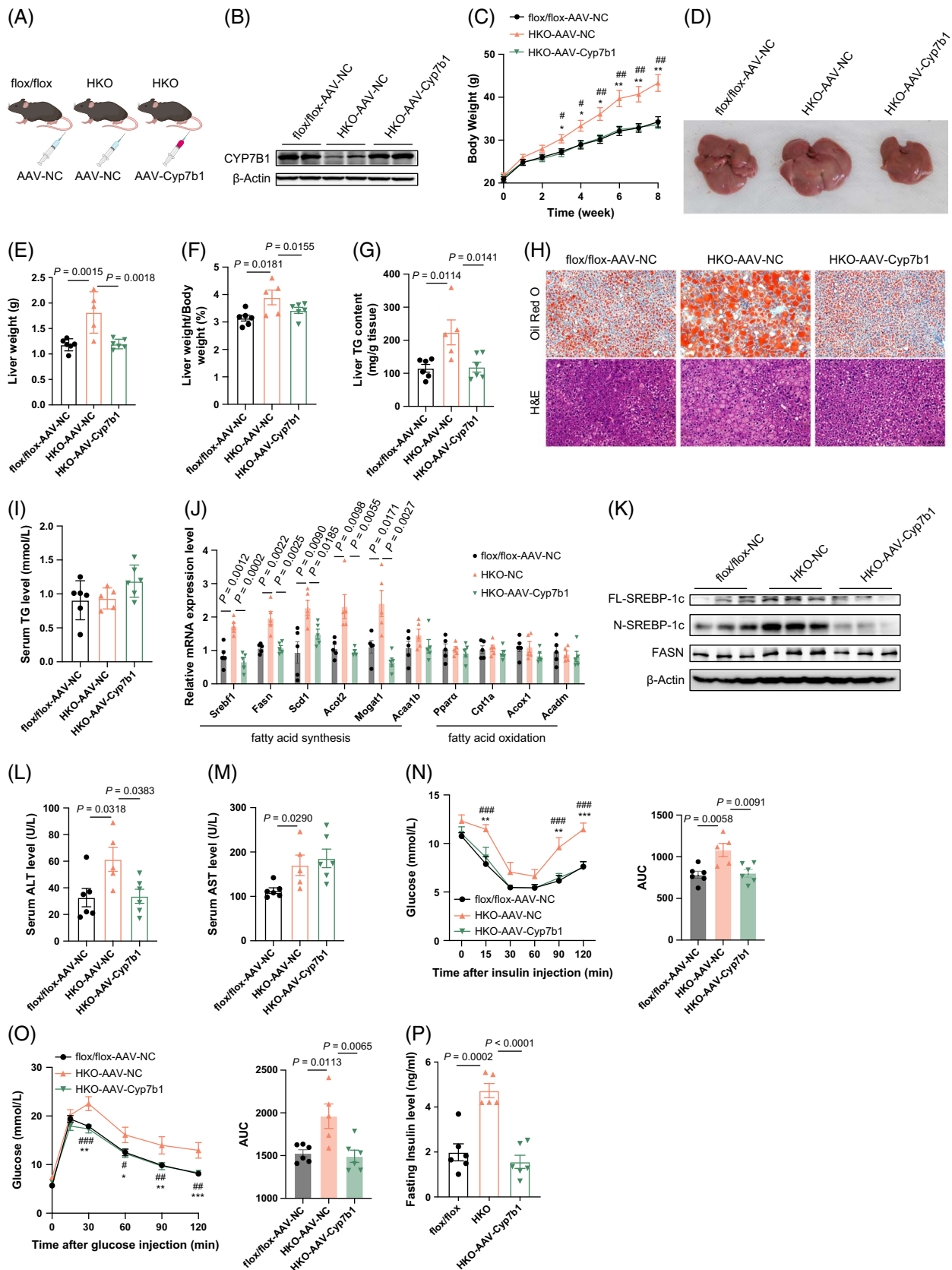
FIGURE 5 CYP7B1 replenishment reverses HFD-induced hepatic steatosis in HKO mice. (A) Schematic diagram of animal experiments. HKO mice were intravenously injected with AAV-*Cyp7b1* (HKO-AAV-*Cyp7b1*) or negative AAV control vector (HKO-AAV-NC), while flox/flox mice were transduced with negative AAV control vector (flox/flox-AAV-NC), all mice were fed a high-fat diet for 7 weeks. (B) Quantitation of protein levels of CYP7B1 in the livers using western blotting. (C) Body weights of mice during a 7-week high-fat diet (n = 5–6). (D) Representative images

of livers (n = 5–6). (E, F) Liver weights (E) and liver-to-body weight ratio (F) (n = 5–6). (G) Hepatic TG contents (n = 5–6). (H) Representative Oil red O (upper panel) and H&E (lower panel) staining of mouse livers (n = 5–6). Scale bar, 100 μm. (I) Serum TG levels (n = 5–6). (J) Relative mRNA expression of genes related to fatty acid synthesis and oxidation in the livers of mice assessed using qPCR (n = 5). (K) Protein levels of lipogenic genes in the liver (n = 3). (L, M) Serum ALT (L) and AST (M) levels (n = 5–6). (N, O) Insulin tolerance test (N), glucose tolerance test (O), and the calculation of the AUC (n = 5–6). (P) Fasting serum insulin level (n = 5–6). Data are presented as mean ± SEM. For (C), (N, left panel), and (O, left panel), significance was determined by two-way ANOVA. For (J), significance was determined by Student's two-tailed t-test. For (E–G), (I), (K), (L), (M), (N, right panel), (O, right panel), and (P), significance was determined by one-way ANOVA. *p < 0.05, **p < 0.01, ***p < 0.001, #p < 0.05, ##p < 0.01, ###p < 0.001 as indicated. *Comparison of flox/flox-AAV-NC and HKO-AAV-NC; #Comparison of HKO-AAV-NC and HKO-AAV-$Cyp7b1$. Abbreviations: AAV, adeno-associated virus; CYP7B1, oxysterol 7 alpha-hydroxylase; H&E, hematoxylin and eosin; HFD, high-fat diet; HKO, hepatocyte-specific $Il22ra1$ knockout; NC, negative control; Srebf1, sterol regulatory element binding transcription factor 1; TG, triglyceride.

mice exhibited lower serum ALT levels than HKO-AAV-NC mice (Figure 5L), alongside improved insulin sensitivity (Figure 5N), glucose tolerance (Figure 5O), and decreased serum insulin levels following CYP7B1 overexpression (Figure 5P), while serum TG and AST levels remained unaltered (Figure 5I and M). These data confirm that CYP7B1 overexpression reversed hepatic steatosis, improved insulin sensitivity, and glucose tolerance in HKO mice.

The 3β HCA accumulation caused by CYP7B1 depletion accelerates lipogenesis in mouse primary hepatocytes and human liver organoids

CYP7B1 is a key enzyme in cholesterol metabolism and oxysterol production.[10] We studied its impact on hepatic steatosis in HKO mice. Oxysterol analysis of the liver tissues from flox/flox and HKO mice revealed distinct separation by principal component analysis (Supplemental Fig. S4A, http://links.lww.com/HEP/I538). In the HKO mice liver, 3β HCA, derived from converting 27-hydroxycholesterol by sterol 27-hydroxylase (CYP27A1) in the cholesterol metabolic process, exhibited the most substantial elevation among various oxysterols compared to flox/flox mice (Figure 6B, Supplemental Fig. S4B, http://links.lww.com/HEP/I538). 3β HCA can be further converted to 3 beta,7 alpha-dihydroxy-5-cholestenoic acid by CYP7B1 (Figure 6A). Treatment of MPHs with 3β HCA led to dose-independent increases in cellular TG (Figure 6D), as confirmed by Oil Red O staining (Figure 6C), attributed to increased expression of lipogenic genes (Figure 6E). Similarly, human liver organoids (HLOs) displayed enhanced lipogenesis when exposed to 3β HCA, as evidenced by Bodipy staining and western blots (Figure 6F and G). IL-22 treatment markedly attenuated lipid synthesis induced by 3β HCA in HLOs (Figure 6F and G). Importantly, MPHs from flox/flox mice treated with 3β HCA showed comparable cellular lipid deposition levels with HKO-derived MPHs (Supplemental Fig. S4C–E, http://links.lww.com/HEP/I538).

The cholesterol metabolic pathway converts cholesterol to oxysterols, which generate bile acids.[16] Bile acids profoundly affect multiple metabolic pathways,

including lipid and glucose metabolism.[17] We analyzed serum bile acids in hepatic IL22RA1-deficient and IL-22-overexpressing mice to explore their role in lipid metabolism regulation. The primary bile acid composition (Supplemental Fig. S5A, http://links.lww.com/HEP/I539), total levels (Supplemental Fig. S5B, http://links.lww.com/HEP/I539), relative abundances of primary and secondary bile acids (Supplemental Fig. S5C, http://links.lww.com/HEP/I539), conjugated and unconjugated bile acids (Supplemental Fig. S5D, http://links.lww.com/HEP/I539), and 12OH and non-12OH bile acids in the serum were comparable between the HFD-fed flox/flox and HKO mice (Supplemental Fig. S5E, http://links.lww.com/HEP/I539). IL-22 treatment minimally affected serum primary bile acid composition and levels in both CD-fed and HFD-fed mice (Supplemental Fig. S5F–J, http://links.lww.com/HEP/I539). These results indicate that increased hepatic oxysterol, particularly 3β HCA, rather than bile acids, may contribute to the detrimental effects observed in hepatic IL22RA1-deficient mice.

LXRs, particularly LXR-alpha ($Nr1h3$), are pivotal oxysterol targets.[10] To investigate if 3β HCA modulates fatty acid synthesis through LXR-alpha binding, a dual luciferase reporter assay was conducted to assess its ability to transactivate the mice sterol regulatory element binding transcription factor 1 ($Srebf1$) gene promoter. LXR-alpha interacts with the retinoid X receptor alpha, forming a heterodimer that binds to the LXR response element and controls gene expression.[10] Through the introduction of LXR-alpha and retinoid X receptor-alpha expression plasmids along with the $Srebf1$ (the target gene of LXR-alpha) reporter plasmid into HEK293T and Hepa 1-6 cells, we observed 3β HCA inducing LXR-alpha transactivation in both cell lines (Figure 6H and I), comparable to the synthetic LXR-alpha agonist T0901317. Additionally, surface plasmon resonance/Biacore analysis demonstrated 3β HCA has a robust affinity (KD = 9.60E-6) for human LXR-alpha (Figure 6J), surpassing the affinity of T0901317 (KD = 8.36E-4) (Supplemental Fig. S5K, http://links.lww.com/HEP/I539).

To assess whether LXR-alpha was indispensable for the lipogenic effect of 3β HCA, we treated the MPHs with SR9243, an LXR-alpha antagonist. SR9243 abolished 3β HCA's promotion of fatty acid synthesis, as evidenced by reducing lipogenic proteins (Figure 6K), lipid droplets (Figure 6L), and cellular TG contents
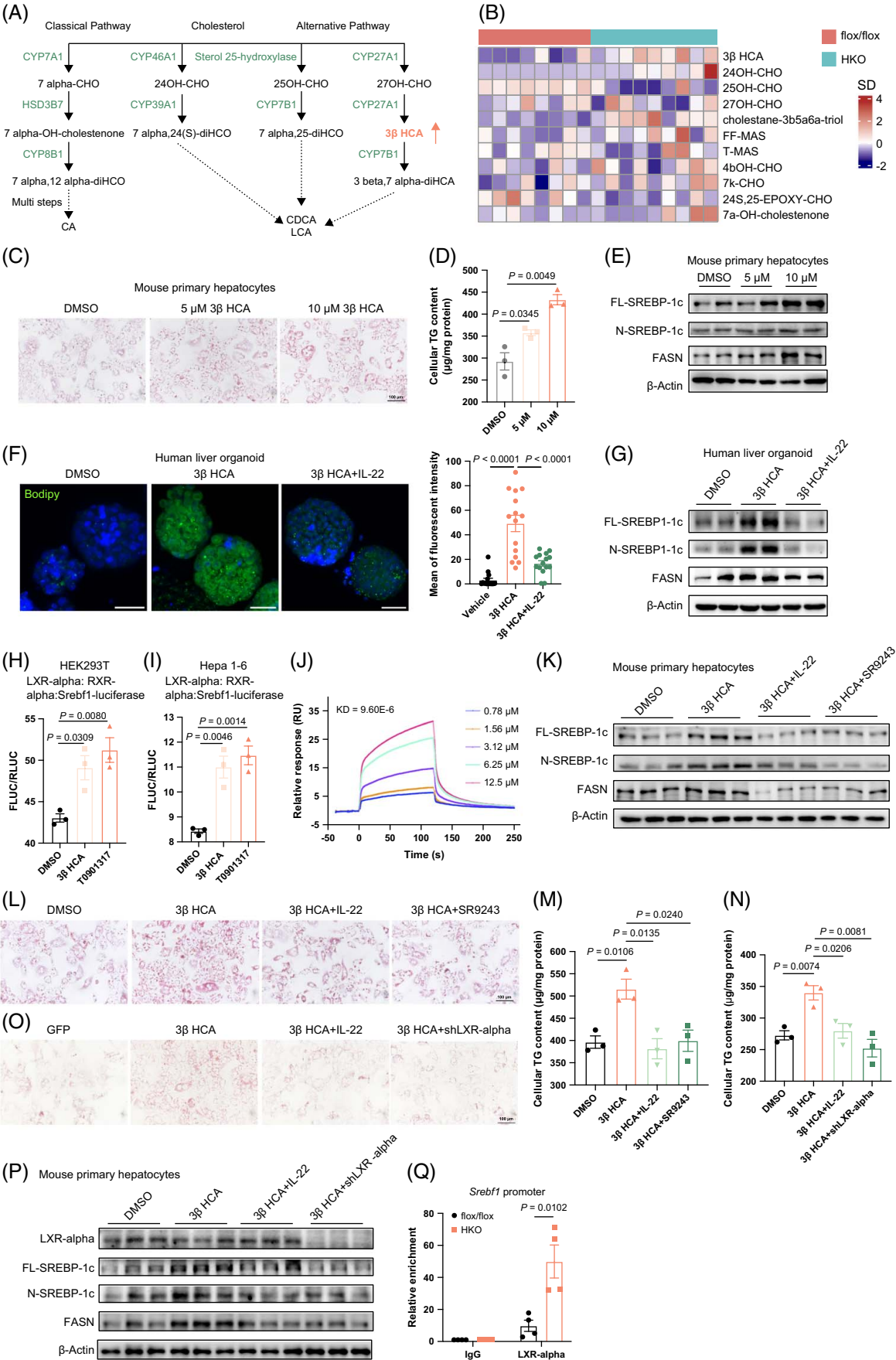
FIGURE 6   The 3β HCA accumulation caused by CYP7B1 depletion accelerates lipogenesis in mouse primary hepatocytes and human liver organoids. (A) Diagram of oxysterol synthesis in hepatocytes. Red arrows indicate higher oxysterol levels found in the liver of HKO mice compared with flox/flox mice. Enzymes are written in blue. (B) Heatmap showing oxysterols in the livers of flox/flox and HKO mice as quantified using LC-MS/MS (n = 8–9). (C–E) MPHs were treated with vehicle DMSO, 5 μM 3β HCA, and 10 μM 3β HCA, and the metabolic phenotype was measured. (C) Representative images of Oil Red O staining of primary mouse hepatocytes treated with different doses of 3β HCA for 24 h (n = 3). Scale bar, 100 μm. (D) Ex vivo cellular TG content in mouse primary hepatocytes after being treated with 3β HCA for 24 h (n = 3). (E) The protein levels of genes involved in fatty acid synthesis were determined using western blotting in mouse primary hepatocytes treated with 3β HCA (n = 2). (F, G) HLOs were administrated with DMSO (Vehicle), 10 μM 3β HCA or 10 μM 3β HCA + 200 ng/mL IL-22 (20-min pretreatment), and metabolic phenotypes were measured. (F) Representative images of lipid droplets in the HLOs (Bodipy in green, and DAPI in blue), and the mean Bodipy fluorescent intensity was quantified (n = 15). Scale bars, 50 μm. (G) Protein levels of lipogenic genes. (H, I) Luciferase assays for the *Srebf1* (the gene harboring the liver X receptor alpha-responsive elements) activity in HEK293T (H) and Hepa1-6 cell lines (I) treated with 10 μM 3β HCA for 24 h. The synthetic LXR-alpha agonist T0901317 (5 μM) was used as a positive control (n = 3). (J) A representative SPR response from the association and dissociation of 3β HCA with human recombinant LXR-alpha. (K–M) MPHs were isolated from 8-week-old C57BL/6J mice and administrated with DMSO (Vehicle, with a final concentration of 0.1%), 10 μM 3β HCA, 10 μM 3β HCA + 100 ng/mL IL-22 (20-min pretreatment), and 10 μM 3β HCA + 20 μM SR9243 (LXR-alpha inhibitor, 2-h pretreatment). (K) Protein levels of the genes associated with fatty acid synthesis in mouse primary hepatocytes (n = 3). (L) Representative images of Oil Red O staining of mouse primary hepatocytes (n = 3). Scale bar, 100 μm. (M) TG contents in mouse primary hepatocytes (n = 3). (N–P) MPHs isolated from C57BL/6J were treated with DMSO (Vehicle, with a final concentration of 0.1%), 10 μM 3β HCA, 10 μM 3β HCA + 100 ng/mL IL-22 (20-min pretreatment), and 10 μM 3β HCA + shLXR-alpha (shRNA was used to silence LXR-alpha expression, 24 h pretreatment). (N) Cellular TG contents (n = 3). (O) Oil Red O staining of MPHs (n = 3). Scale bar, 100 μm. (P) The protein levels of LXR-alpha and its target genes were measured using western blotting (n = 3). (Q) ChIP-qPCR assay showing recruitment of LXR-alpha onto the promoter region of *Srebf1* (n = 4). Data are presented as mean ± SEM. For (D), (H), (I), and (F, right panel), significance was determined by one-way ANOVA. For (M), (N), and (Q), significance was determined using the Student two-tailed *t*-test. Abbreviations: 7 alpha-CHO, 7alpha-hydroxycholesterol; 24OH-CHO, 24-hydroxycholesterol; 25OH-CHO, 25-hydroxycholesterol; 27OH-CHO, 27-hydroxycholesterol; 7 alpha-OH-cholestenone, 7 alpha-hydroxy-4-cholesten-3-one; 7 alpha,24(S)-diHCO, 7 alpha,24(S)-dihydroxycholesterol; 7 alpha,25-diHCO, 7 alpha,25-dihydroxycholesterol; 3β HCA, 3 beta-hydroxy-5-cholestenoic Acid; 7 alpha,12 alpha-diHCO, 7 alpha-12 alpha-dihydroxy-4-cholesten-3-one; 3 beta,7 alpha-diHCA, 3 beta,7 alpha-dihydroxy-5-cholestenoic acid; CYP7A1, cholesterol 7 alpha-hydroxylase; ChIP, chromatin immunoprecipitation; CYP27A1, sterol 27-hydroxylase; CYP39A1, sterol 7 alpha-hydroxylase; CYP46A1, sterol 24-hydroxylase; CYP7B1, oxysterol 7 alpha-hydroxylase; CYP8B1, sterol-12 alpha-hydroxylase; FLUC/RLUC, firefly luciferase to renilla luciferase ratio; HEK293T, human embryonic kidney 293t; HKO, hepatocyte-specific Il22ra1 knockout; HLOs, human liver organoids; HSD3B7, 3 beta-hydroxysteroid dehydrogenase; LC-MS/MS, liquid chromatography-tandem mass spectrometry; LXR-alpha, liver X receptor alpha; MPHs, mouse primary hepatocytes; SPR, surface plasmon resonance; Srebf1, sterol regulatory element binding transcription factor 1; SREBP, sterol regulatory element binding protein; TG, triglycerides.

(Figure 6M). The effect of IL-22 on abrogating 3β HCA-driven lipogenesis mirrored that of SR9243 (Figure 6K–M). Adenovirus-mediated LXR-alpha knockdown further confirms these findings, demonstrating silencing LXR-alpha counteracted lipogenesis induced by 3β HCA (Figure 6N–P). Additionally, chromatin immunoprecipitation assays showed elevated recruitment of LXR-alpha to *Srebf1* promoter regions in the livers of HKO mice compared to flox/flox mice (Figure 6Q). These findings collectively indicated that LXR-alpha was essential for 3β HCA-induce lipogenesis.

ATF3 represses *Cyp7b1* expression in the liver of HKO mice

Subsequently, we probed the upstream regulator of CYP7B1 and found that small heterodimer partner, an atypical nuclear receptor encoded by *Nr0b2* influencing *Cyp7b1* expression,[18] remained unchanged after IL-22 overexpression or hepatic IL22RA1 deficiency (Figure 4E–L). Therefore, we analyzed the RNA-seq data globally to identify the potential upstream regulators modulating CYP7B1 expression. After studying differentially expressed transcription factors in CD-fed, HFD-fed IL-22 overexpression, and HKO mice, we pinpointed 4 overlapping transcription factors across the models: *Atf3*, *Srebf1*, *Nrli2*, and *Zbtb7c*

(Figure 7A and B). Among these, *Atf3* and *Srebf1* displayed contrasting gene expression patterns in CD-fed and HFD-fed IL-22 overexpression versus HKO mice. *Nr1i2* and *Zbtb7c*, the 2 other transcription factors, exhibited contrasting trends between the CD-fed and HFD-fed IL-22 overexpression models. Given IL-22's ability to reduce hepatic TG accumulation under both CD (Supplemental Fig. S1, http://links.lww.com/HEP/I535) and HFD conditions (Figure 1), we postulated that target transcription factors expression would reflect similar trends. Other studies linked ATF3 to hepatic steatosis.[19–21] In this study, western blots analysis showed IL-22 lowering ATF3 expression in HFD-fed mice while boosting CYP7B1 expression (Figure 7C). In contrast, ATF3 levels increased while CYP7B1 decreased in the liver of HFD-fed HKO mice compared to the flox/flox mice (Figure 7D). Luciferase reporter assays confirmed that ATF3 repressed CYP7B1 expression (Figure 7E). Consistently, analyzing public transcriptome data[14] (GSE135251) comprising 206 liver biopsies from patients with NAFLD revealed a significantly negative correlation between *ATF3* and *CYP7B1* mRNA expression (Figure 7F). These data shed light on how ATF3 acts as a transcriptional suppressor of CYP7B1 in the liver.

IL-22 primarily activates the Janus kinase/STAT pathway.[5] Therefore, we determined whether STAT3 is directly upstream of *Atf3* using luciferase reporter assays and revealed the negative regulatory effects of
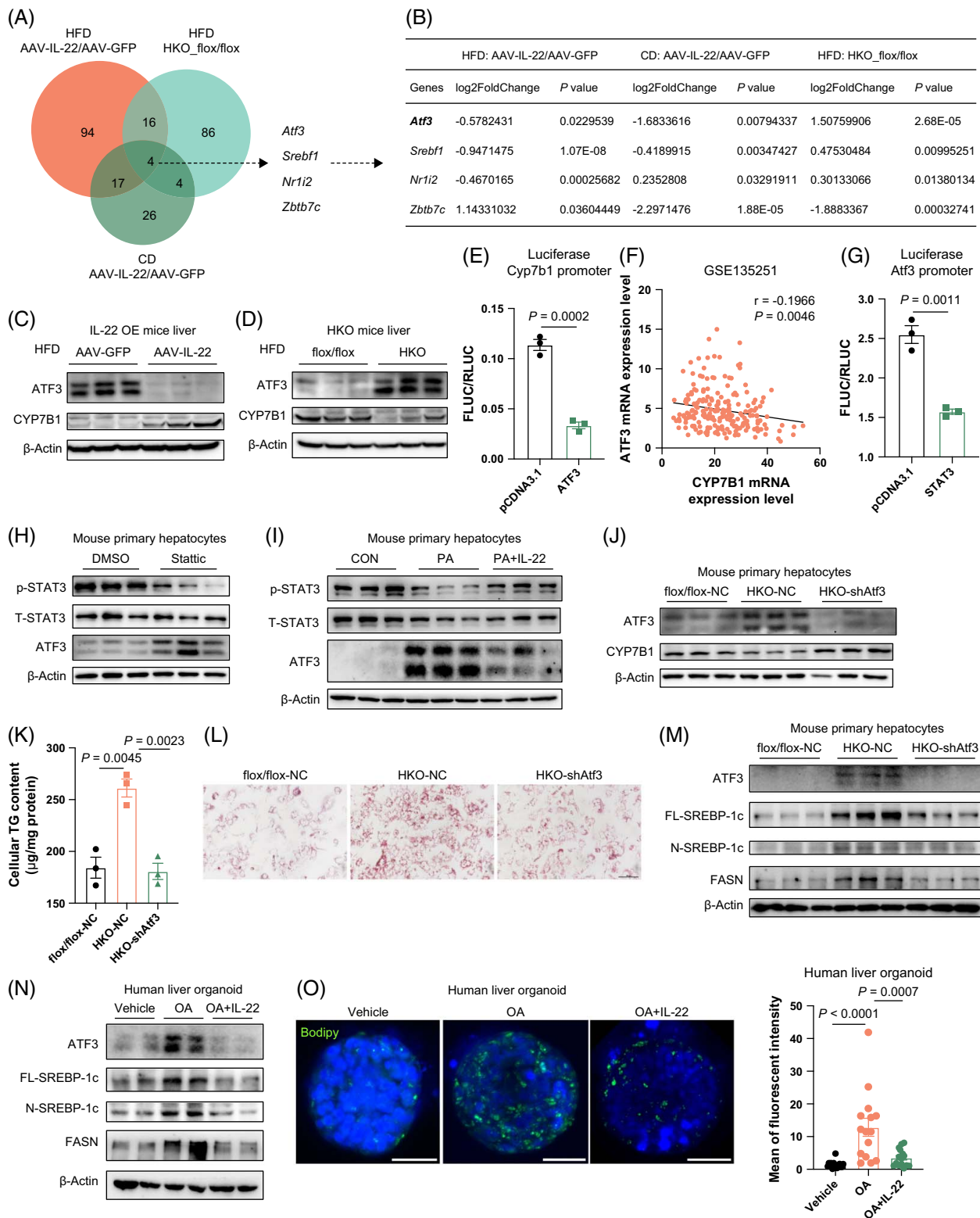
FIGURE 7 Activating transcription factor 3 (ATF3) negatively regulates *Cyp7b1* expression in the liver of HKO mice. (A) A Venn diagram of transcription factors that were differentially expressed ($p < 0.05$) showed opposite changes in the livers of AAV-IL-22 and HKO mice, as identified using RNA-seq. (B) A list showing the 4 overlap genes generated from the 3 pairs of compare analyses, including CD-fed and HFD-fed AAV-IL-22 versus AAV-GFP, HFD-fed HKO versus flox/flox. Protein levels of ATF3 and CYP7B1 in the livers of HFD-fed AAV-IL-22 and AAV-GFP mice (n = 3) (C), and HFD-fed flox/flox and HKO mice (n = 3) (D). (E) The *Cyp7b1* promoter, regulated by ATF3, was measured using a luciferase assay in HEK293T cells (n = 3). (F) Analysis of public transcriptome data (GSE135251) comprising 206 liver biopsies from patients with NAFLD revealed a negative association of *ATF3* with *CYP7B1* in individuals with NAFLD. (G) The *Atf3* promoter, regulated by signal transducer and activator of transcription 3 (STAT3), was measured using a luciferase assay in HEK293T cells (n = 3). (H) MPHs isolated from C57BL/6J mice were treated

with stattic (10 μM, inhibitor of p-STAT3) for 4 h, phosphor-STAT3 (p-STAT3), total-STAT3 (T-STAT3), and ATF3 levels were quantified using western blotting; a 24-hour treatment of MPHs was applied for western blotting analysis of ATF3 and CYP7B1 protein levels (n = 3). (I) MPHs isolated from C57BL/6J mice were treated with 10% BSA (Vehicle, with a final concentration of 0.5%), PA (final concentration 0.25 mM), and PA + 100 ng/mL IL-22 (20 min pretreatment). Phosphor-STAT3 (p-STAT3) and total-STAT3 (T-STAT3) levels and ATF3 were assessed using western blotting. A 24-hour treatment of MPHs with PA and IL-22 was used for western blotting detection of ATF3 and CYP7B1 protein levels (n = 3). (J– M) shRNA was used to knock down ATF3 in MPHs from HKO mice ex vivo. (J) ATF3 and CYP7B1 protein levels in MPHs from flox/flox and HKO mice (n = 3). (K) Cellular TG contents (n = 3). (L) Representative images of Oil Red O staining of the MPHs (n = 3). Scale bar, 100 μm. (M) The protein levels of ATF3 and genes involved in fatty acid synthesis were quantified using western blotting (n = 3). (N, O) HLOs were administrated with BSA (Vehicle), 0.5 mM oleic acid (OA) or 0.5 mM OA + 200 ng/mL IL-22 (20-min pretreatment), and metabolic phenotypes were measured. (N) Protein levels of ATF3 and lipogenic genes. (O) Representative images of lipid droplets in the HLOs (Bodipy in green and DAPI in blue), and the mean Bodipy fluorescent intensity was quantified (n = 15). Scale bars, 50 μm. Data are presented as mean ± SEM. For (E) and (G), significance was determined using the Student two-tailed *t*-test. For (K) and (O, right panel), significance was determined by one-way ANOVA. Abbreviations: AAV, adeno-associated virus; ATF3, activating transcription factor 3; BSA, bovine serum albumin; CD, chow diet; CYP7B1, oxysterol 7 alpha-hydroxylase; FLUC/RLUC, firefly luciferase to renilla luciferase ratio; GFP, green fluorescent protein; HFD, high-fat diet; HKO, hepatocyte-specific *Il22ra1* knockout; HLOs, human liver organoids; OA, oleic acid; PA, palmitic acid; Srebf1, sterol regulatory element binding transcription factor 1; STAT3, signal transducer and activator of transcription 3; TG, triglyceride.

STAT3 on ATF3 expression in HEK293T cells (Figure 7G). Inhibiting p-STAT3 levels using stattic, a specific inhibitor, increased ATF3 protein levels in MPHs (Figure 7H), leading to enhanced lipid accumulation (Supplemental Fig. S6A and B, http://links.lww.com/HEP/I540), primarily by facilitating the expression of lipogenic genes (Supplemental Fig. S6C and D, http://links.lww.com/HEP/I540). Notably, IL-22 treatment reversed the downregulation of p-STAT3 levels and dampened ATF3 expression induced by PA treatment (Figure 7I). This suggests that IL-22 modifies lipid homeostasis in hepatocytes by inhibiting ATF3 through STAT3, providing metabolic benefits during high-energy diet conditions.

To illustrate the role of ATF3 in HKO mice, we introduced an adenovirus-interfering mouse *Atf3* expression into MPHs from HKO mice. ATF3 knockdown increased CYP7B1 expression (Figure 7J), attenuated cellular TG content (Figure 7K), and diminished lipid droplet accumulation (Figure 7L), mainly by decreasing lipogenic protein expression in MPHs derived from HKO mice (Figure 7M). This suggests that dampening ATF3 restored CYP7B1 expression, reducing lipid accumulation in HKO mice-derived MPHs. Treating HLOs with oleic acid raised ATF3 levels and lipogenic gene expression. However, IL-22 counteracted oleic acid's effects by suppressing ATF3 expression in HLOs (Figure 7N and O).

ATF3 knockdown in the liver of HKO mice attenuates hepatic steatosis and improves glucose homeostasis

To evaluate the lipid regulatory effect of ATF3 in HKO mice, we used AAV8 to deplete ATF3 expression in the liver (Figure 8A). ATF3 depletion increased CYP7B1 expression (Figure 8B), reduced body weights (Figure 8C), liver weights (Figure 8D and E), and liver-to-body weight ratio in HKO mice (Figure 8F). This

depletion mitigated steatosis in the liver of HKO-sh*Atf3* mice without affecting serum TG levels (Figure 8G–K). Decreased serum ALT and AST levels were observed (Figure 8L and M), indicating reduced liver damage in HKO-sh*Atf3* mice compared with HKO-NC mice. Moreover, ATF3 knockdown improved insulin sensitivity and glucose tolerance (Figure 8N and O), with reduced fasting insulin levels in HKO-sh*Atf3* mice (Figure 8P). These results demonstrate that ATF3 interference restored CYP7B1 expression, alleviating hepatic steatosis and improving glucose homeostasis. Notably, both ATF3 knockdown and CYP7B1 overexpression in HKO mice reduced hepatic 3β HCA contents to levels similar to those in flox/flox mice (Figure 8Q and R).

DISCUSSION

IL-22 signaling plays a role in hepatic lipid homeostasis,[7,8] but the exact molecular mechanisms remained partially elucidated. Our study revealed significant downregulation of IL22RA1 in hepatocytes of murine and individuals with NAFLD, suggesting its importance in hepatic lipid homeostasis. By generating hepatocyte-specific *Il22ra1* knockout mice, we demonstrated that hepatocyte-specific IL22RA1 deficiency accentuated HFD-induced hepatic steatosis, weight gain, glucose intolerance, and insulin resistance on an HFD while also intensifying fibrosis and inflammation on an HFHC diet. Depletion of CYP7B1 expression in the livers of HKO mice led to increased 3β HCA levels, enhancing lipogenesis through LXR-alpha activation. IL-22 treatment reduced the lipogenic effects of 3β HCA in both MPHs and HLOs, suggesting potential therapeutic implications in humans. Mechanistically, we identified the ATF3-CYP7B1 axis as crucial for hepatic lipid homeostasis in HKO mice. In summary, our findings elucidate the precise molecular mechanisms controlling hepatic lipid metabolism in hepatocyte-specific IL22RA1-deficient mice, highlighting the novel role of 3β HCA in modulating lipogenesis.
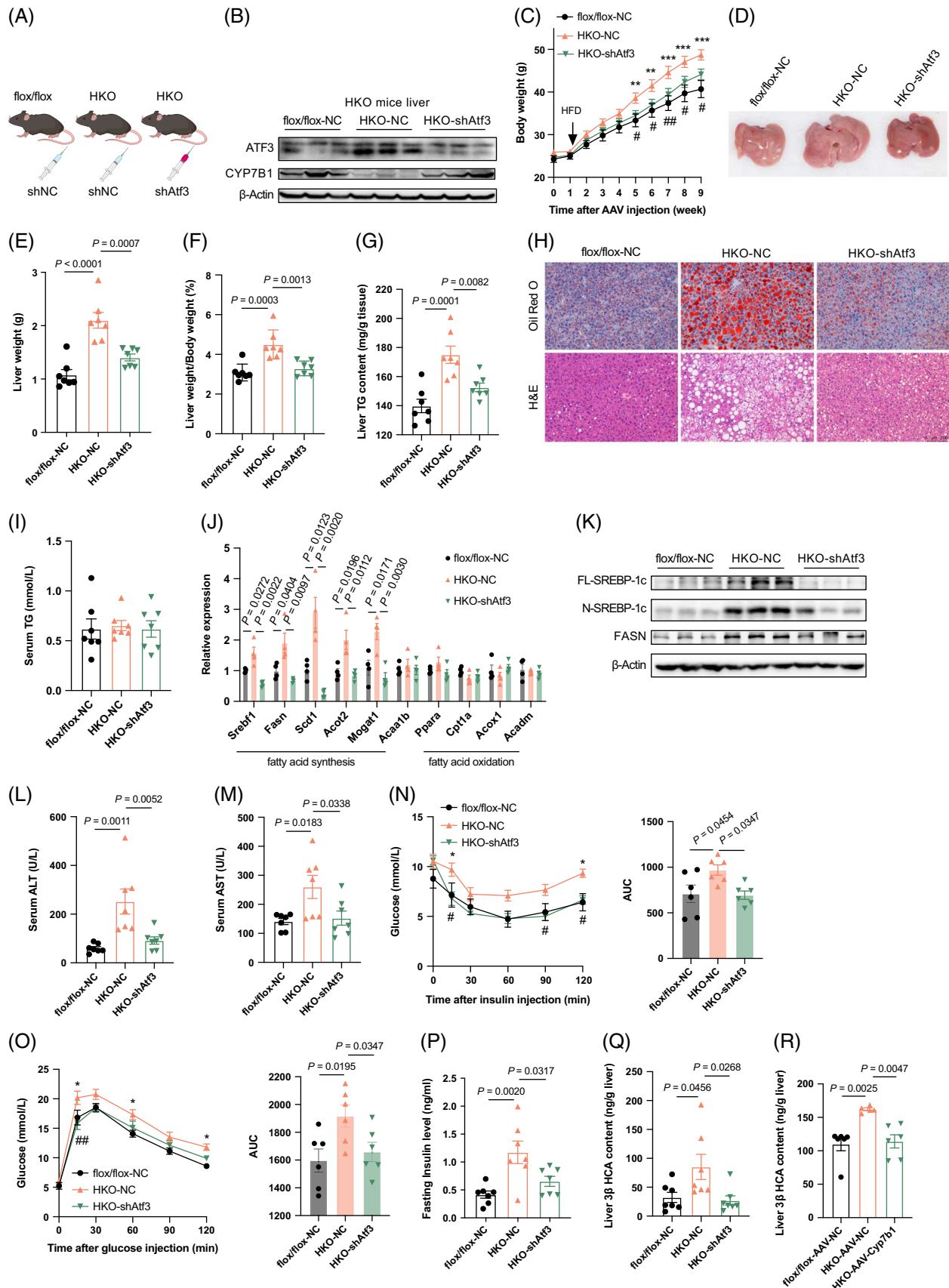
FIGURE 8 ATF3 silencing in the liver of HKO mice attenuates hepatic steatosis and improves glucose homeostasis. (A) Schematic diagram of animal experiments. HKO mice were injected with AAV-shAtf3 (HKO-shAtf3) or AAV negative control vector (HKO-NC) through the tail vein, flox/flox mice were i.v. injected with the AAV negative control vector, and the metabolic phenotype was assessed. (B) ATF3 and

CYP7B1 protein levels in whole liver lysates (n = 3). (C) Body weights of mice on an 8-week HFD (n = 10). (D) Representative image of livers. (E, F) Liver weights (E) and liver-to-body weight ratio (F) (n = 7). (G) Liver TG contents (n = 7). (H) Oil Red O (upper panel) and H&E staining (lower panel) of liver sections were reviewed in 6 mice per group. Scale bar, 100 μm. (I) Serum TG levels (n = 7). (J) Relative mRNA expression of genes associated with fatty acid synthesis and oxidation in the liver (n = 4). (K) Protein levels of lipogenic genes in the whole liver lysate (n = 3). (L, M) Serum levels of ALT (L) and AST (M) (n = 7). (N, O) Insulin tolerance test (N), glucose tolerance test (O), and the calculated AUC of (n = 6). (P) Fasting serum insulin levels (n = 7). (Q) Hepatic 3β HCA content of mice in the indicated group (n = 7). (R) Hepatic 3β HCA content of mice in the indicated group (n = 5–6). Data are presented as mean ± SEM. For (C), (N, left panel), and (O, left panel), significance was determined using the two-way ANOVA. For (E–G), (L), (N, right panel), (O, right panel), and (P–R), significance was determined by one-way ANOVA. For (J), significance was determined by Student two-tailed t-test. *p < 0.05, **p < 0.01, ***p < 0.001, #p < 0.05, ##p < 0.01, ###p < 0.001 as indicated. *Comparison of flox/flox-NC and HKO-NC; #Comparison of HKO-NC and HKO-shAtf3. Abbreviations: AAV, adeno-associated virus; ATF3, activating transcription factor 3; CYP7B1, oxysterol 7 alpha-hydroxylase; 3β HCA, 3 beta-Hydroxy-5-cholestenoic Acid; H&E, hematoxylin and eosin; HFD, high-fat diet; HKO, hepatocyte-specific *Il22ra1* knockout; Srebf1, sterol regulatory element binding transcription factor 1; TG, triglyceride.

The regulatory role of IL22RA1 in hepatic lipid metabolism seems controversial. Gaudino et al observed no significant differences in hepatic histology or lipid deposition between hepatocyte-specific IL22RA1 knockout and control mice fed an HFD.[22] In contrast, our study reported that hepatocyte-specific IL22RA1 ablation aggravates hepatic fat accumulation under HFD conditions. Discrepancies may stem from distinct strategies used to generate the floxed *Il22ra1* allele: we used loxP sites flanking exon 2, while Gaudino et al targeted exon 3. Different knockout strategies result in diverse protein truncations, potentially causing distinct effects. For instance, diverse liver METTL3 knockout approaches yield different phenotypes. Studies using different Mettl3-floxed mouse lines showed that targeting 4[23] or exon 2–4[24] led to liver development defects while targeting exons 2–3 did not.[25] These discrepancies underscore the significant impact of potential protein products resulting from targeted gene exon deletions, which is crucial for accurately interpreting phenotypes.

IL22RA1 expression in metabolically associated tissues plays distinct regulatory roles. Intestinal epithelium-specific IL22RA1 knockout impairs systemic glucose clearance, increases liver lipid deposition, and promotes inflammation in white adipose tissue without affecting weight gain or insulin sensitivity.[22] Conversely, white adipose tissue-specific IL22RA1 deficiency displays no metabolic disorders under HFD conditions.[22] Pancreatic beta-cell IL22RA1 deficiency decreases insulin secretion, quality, and islet regeneration.[26] In our study, hepatocyte-specific IL22RA1 knockout results in weight gain, impairs glucose tolerance and insulin sensitivity, and worsens NAFLD progression in mice. This suggests that IL22RA1 controls metabolism in a context-dependent manner.

Various studies, including ours, demonstrate that IL-22 ameliorates hepatic steatosis in obese mice.[7,8] Despite reduced hepatic IL22RA1 protein levels after an HFD, IL-22 effectively mitigated hepatic steatosis. This could be attributed to the partial downregulation, not complete elimination of IL22RA1 expression in the liver, which allows for sufficient transmission of IL-22 signals.

Furthermore, overexpression of IL-22 raised serum IL-22 levels beyond normal physiological levels (30–100 pg/mL), indicating that a dosage closer to the physiological range (~300 pg/mL) might enhance its effects further. Likewise, AdipoR2, the predominant receptor for adiponectin in the liver, is downregulated in NAFLD and NASH.[27] However, studies have confirmed that adiponectin treatment can still alleviate NAFLD.[28,29]

In our RNA-seq analysis, we observed varying ATF3 expression in the liver of HKO and IL-22 overexpression mice. ATF3, a stress-induced transcription factor crucial for metabolism regulation, displayed increased levels upon deleting hepatic IL22RA1. Inhibiting ATF3 expression attenuates hepatic steatosis in HKO mice, consistent with findings where ATF3 siRNA administration ameliorated hepatic steatosis in rats.[19] While ATF3 overexpression led to enhanced lipid accumulation, its knockdown alleviates lipid deposition.[20] Conflicting reports[21] suggest that global or hepatocyte-specific ATF3 loss exacerbates HFHC diet-induced hepatic steatosis and steatohepatitis, indicating a protective role for ATF3. ATF3 seems beneficial during early disease stages but potentially harmful if overexpressed chronically. The outcomes of targeting ATF3 expression using different animal models or siRNA approaches vary due to ATF3's context-dependent functions. Balancing ATF3 expression under stress conditions, rather than complete abolishment, may be critical in addressing prolonged HFD-induced obesity-related complications.

Our study revealed that *Cyp7b1* controls hepatic lipids. IL-22 overexpression increased CYP7B1 levels, while IL22RA1 deficiency decreased them. Restoring hepatic CYP7B1 expression reversed steatosis in HKO mice. We observed elevated 3β HCA levels in IL22RA1-deficient mice livers. This oxysterol is generated through a 2-step enzyme reaction catalyzed by sterol 27-hydroxylase (CYP27A1) and further converted to 3 beta,7 alpha-dihydroxy-5-cholestenoic acid by CYP7B1.[16] The increase in 3β HCA could be attributed to reduced hepatic CYP7B1 levels, as *Cyp27a1* expression remained unaltered. Similarly, patients with CYP7B1 deficiency exhibited early-life 3β HCA accumulation, leading to severe neonatal liver disease

caused by bile acid metabolic dysfunction.[30] Notably, liver 3β HCA contents increased in a time-dependent manner during a 6-week western diet in a mouse model, correlating this rise with increased hepatic inflammation and injury.[31]

In this study, we found that 3β HCA promotes lipogenesis in MPHs by binding to LXR-alpha. This pro-lipogenic effect was validated using a human pluripotent stem cells induced HLOs model, resembling human organ functions. Importantly, 3β HCA activated LXR-alpha comparably to the synthetic LXR-alpha agonist T0901317, emphasizing its lipogenic properties. IL-22 effectively attenuated 3β HCA's lipogenic function in both MPHs and HLOs. Our findings highlight the significance of liver oxysterols, specifically 3β HCA, in regulating hepatic lipids. Oxysterols are crucial for metabolism modulation. For instance, administering 25HC has been found to alleviate steatosis in mice.[12] Impairment of oxysterol balance contributes to conditions like atherogenesis and inflammation.[32]

NAFLD presents diverse therapeutic avenues under clinical investigation to target steatosis, inflammation, and fibrosis.[33] Combining or using single medications addressing multiple aspects could yield superior outcomes.[33] IL-22 emerges as a promising candidate with anti-steatotic, anti-inflammatory, and anti-fibrotic effects in the liver. Evidence shows IL-22's efficacy in alleviating hepatic steatosis and fibrosis in mouse models.[6–9,34,35] Clinical trials have underscored IL-22's potential in treating NAFLD. Phase I clinical trials indicate that IL-22Fc is well tolerated in healthy individuals, with minimal adverse effects.[36] A phase IIa trial has demonstrated both the safety and efficacy of IL-22Fc in patients with severe alcohol-associated hepatitis.[37] These positive outcomes primarily stem from IL-22/IL22RA1 signaling activation of STAT3 in hepatocytes and HSCs.[7,8,34]

There were several limitations in the present study. First, we noted decreased IL22RA1 expression in NAFLD without an explanation for this downregulation. Second, our study illustrated 3β HCA's lipogenic role in hepatocytes and HLOs but did not fully investigate its effects on inflammatory response. Lastly, while we showed that 3β HCA boosts lipogenic in MPHs and HLOs, further research is needed to determine if similar results occur in vivo, specifically in mice and nonhuman primates.

In conclusion, our data indicated that hepatic IL22RA1 modulates lipid homeostasis through the ATF3/CYP7B1/3β HCA /LXR-alpha signaling. Our study uncovered a new role for 3β HCA as a potent activator of lipogenesis in hepatocytes, potentially accounting for hepatic lipid synthesis in hepatic IL22RA1-deficient mice. IL-22 effectively suppresses the lipogenic effects of 3β HCA, highlighting the therapeutic potential of IL-22/IL22RA1 in NAFLD.

AUTHOR CONTRIBUTIONS

Cheng Hu, Yan Lu, Yeping Huang, and Fan Yu designed the study. Yeping Huang and Fan Yu performed most of the experiments, analyzed the data, and wrote the manuscript. Yue Ding and Min Jiang. measured the hepatic oxysterol content. Hong Zhang analyzed the RNA-seq data and contributed to data interpretation. Xinyue Li and Xiao Wang. assisted with the cellular and animal experiments, tissue collection, qPCR analysis, western blotting analysis, and immunofluorescence imaging. Rong Zhang provided valuable suggestions on this study. Jie Xu, Liang Wang, Chenxu Tian, Guangzhong Xu, Xiao Ye, Chenyan Yan, Yingxiang Song, and Haijun Huang contributed to the collection of liver samples and related clinical information. Xiaoshan Wu and Qiurong Ding conducted the experiments related to human liver organoids. Cheng Hu and Yan Lu supervised the project. All authors have read and approved the final manuscript.

FUNDING INFORMATION

ACKNOWLEDGMENTS

CONFLICTS OF INTEREST

The authors have no conflicts to report.

ORCID

Yan Lu https://orcid.org/0000–0003–3468–2241
Cheng Hu https://orcid.org/0000–0003–4314–2386

REFERENCES

1. Targher G, Lonardo A, Byrne CD. Nonalcoholic fatty liver disease and chronic vascular complications of diabetes mellitus. Nat Rev Endocrinol. 2018;14:99–114.

2. Hodson L, Gunn PJ. The regulation of hepatic fatty acid synthesis and partitioning: The effect of nutritional state. Nat Rev Endocrinol. 2019;15:689–700.

3. Wang Y, Viscarra J, Kim SJ, Sul HS. Transcriptional regulation of hepatic lipogenesis. Nat Rev Mol Cell Biol. 2015;16:678–89.

4. Batchuluun B, Pinkosky SL, Steinberg GR. Lipogenesis inhibitors: Therapeutic opportunities and challenges. Nat Rev Drug Discov. 2022;21:283–305.

5. Dudakov JA, Hanash AM, van den Brink MR. Interleukin-22: Immunobiology and pathology. Annu Rev Immunol. 2015;33:747–85.

6. Zai W, Chen W, Liu H, Ju D. Therapeutic opportunities of IL-22 in non-alcoholic fatty liver disease: From molecular mechanisms to clinical applications. Biomedicines. 2021;9:1912.

7. Wang X, Ota N, Manzanillo P, Kates L, Zavala-Solorio J, Eidenschenk C, et al. Interleukin-22 alleviates metabolic disorders and restores mucosal immunity in diabetes. Nature. 2014;514:237–41.

8. Yang L, Zhang Y, Wang L, Fan F, Zhu L, Li Z, et al. Amelioration of high fat diet induced liver lipogenesis and hepatic steatosis by interleukin-22. J Hepatol. 2010;53:339–47.

9. Hwang S, He Y, Xiang X, Seo W, Kim SJ, Ma J, et al. Interleukin-22 ameliorates neutrophil-driven nonalcoholic steatohepatitis through multiple targets. Hepatology. 2020;72:412–29.

10. Guillemot-Legris O, Mutemberezi V, Muccioli GG. Oxysterols in metabolic syndrome: From bystander molecules to bioactive lipids. Trends Mol Med. 2016;22:594–614.

11. Lu Y, Wang E, Chen Y, Zhou B, Zhao J, Xiang L, et al. Obesity-induced excess of 17-hydroxyprogesterone promotes hyperglycemia through activation of glucocorticoid receptor. J Clin Invest. 2020;130:3791–804.

12. Dong Z, He F, Yan X, Xing Y, Lei Y, Gao J, et al. Hepatic reduction in cholesterol 25-hydroxylase aggravates diet-induced steatosis. Cell Mol Gastroenterol Hepatol. 2022;13:1161–79.

13. Xiao Y, Batmanov K, Hu W, Zhu K, Tom AY, Guan D, et al. Hepatocytes demarcated by EphB2 contribute to the progression of nonalcoholic steatohepatitis. Sci Transl Med. 2023;15:eadc9653.

14. Govaere O, Cockell S, Tiniakos D, Queen R, Younes R, Vacca M, et al. Transcriptomic profiling across the nonalcoholic fatty liver disease spectrum reveals gene signatures for steatohepatitis and fibrosis. Sci Transl Med. 2020;12:eaba4448.

15. Machado MV, Diehl AM. Pathogenesis of nonalcoholic steatohepatitis. Gastroenterology. 2016;150:1769–77.

16. Russell DW. The enzymes, regulation, and genetics of bile acid synthesis. Annu Rev Biochem. 2003;72:137–74.

17. Molinaro A, Wahlstrom A, Marschall HU. Role of bile acids in metabolic control. Trends Endocrinol Metab. 2018;29:31–41.

18. Boulias K, Katrakili N, Bamberg K, Underhill P, Greenfield A, Talianidis I. Regulation of hepatic metabolic pathways by the orphan nuclear receptor SHP. EMBO J. 2005;24:2624–33.

19. Kim JY, Park KJ, Hwang JY, Kim GH, Lee D, Lee YJ, et al. Activating transcription factor 3 is a target molecule linking hepatic steatosis to impaired glucose homeostasis. J Hepatol. 2017;67:349–59.

20. Tu C, Xiong H, Hu Y, Wang W, Mei G, Wang H, et al. Cardiolipin synthase 1 ameliorates NASH through activating transcription factor 3 transcriptional inactivation. Hepatology. 2020;72:1949–67.

21. Xu Y, Hu S, Jadhav K, Zhu Y, Pan X, Bawa FC, et al. Hepatocytic activating transcription factor 3 protects against steatohepatitis via hepatocyte nuclear factor 4alpha. Diabetes. 2021;70:2506–17.

22. Gaudino SJ, Singh A, Huang H, Padiadpu J, Jean-Pierre M, Kempen C, et al. Intestinal IL-22RA1 signaling regulates intrinsic and systemic lipid and glucose metabolism to alleviate obesity-associated disorders. Nat Commun. 2024;15:1597.

23. Wang S, Chen S, Sun J, Han P, Xu B, Li X, et al. m(6)A modification-tuned sphingolipid metabolism regulates postnatal liver development in male mice. Nat Metab. 2023;5:842–60.

24. Xu Y, Zhou Z, Kang X, Pan L, Liu C, Liang X, et al. Mettl3-mediated mRNA m(6)A modification controls postnatal liver development by modulating the transcription factor Hnf4a. Nat Commun. 2022;13:4555.

25. Li X, Yuan B, Lu M, Wang Y, Ding N, Liu C, et al. The methyltransferase METTL3 negatively regulates nonalcoholic steatohepatitis (NASH) progression. Nat Commun. 2021;12:7213.

26. Sajiir H, Wong KY, Müller A, Keshvari S, Burr L, Aiello E, et al. Pancreatic beta-cell IL-22 receptor deficiency induces age-dependent dysregulation of insulin biosynthesis and systemic glucose homeostasis. Nat Commun. 2024;15:4527.

27. Kaser S, Moschen A, Cayon A, Kaser A, Crespo J, Pons-Romero F, et al. Adiponectin and its receptors in non-alcoholic steatohepatitis. Gut. 2005;54:117–21.

28. Jiménez-Castro MB, Casillas-Ramírez A, Mendes-Braz M, Massip-Salcedo M, Gracia-Sancho J, Elias-Miró M, et al. Adiponectin and resistin protect steatotic livers undergoing transplantation. J Hepatol. 2013;59:1208–14.

29. Xu A, Wang Y, Keshaw H, Xu LY, Lam KS, Cooper GJ. The fat-derived hormone adiponectin alleviates alcoholic and nonalcoholic fatty liver diseases in mice. J Clin Invest. 2003;112:91–100.

30. Setchell KD, Schwarz M, O'Connell NC, Lund EG, Davis DL, Lathe R, et al. Identification of a new inborn error in bile acid synthesis: Mutation of the oxysterol 7alpha-hydroxylase gene causes severe neonatal liver disease. J Clin Invest. 1998;102:1690–703.

31. Kakiyama G, Marques D, Martin R, Takei H, Rodriguez-Agudo D, LaSalle SA, et al. Insulin resistance dysregulates CYP7B1 leading to oxysterol accumulation: A pathway for NAFL to NASH transition. J Lipid Res. 2020;61:1629–44.

32. Canfrán-Duque A, Rotllan N, Zhang X, Andrés-Blasco I, Thompson BM, Sun J, et al. Macrophage-derived 25-hydroxycholesterol promotes vascular inflammation, atherogenesis, and lesion remodeling. Circulation. 2023;147:388–408.

33. Harrison SA, Allen AM, Dubourg J, Noureddin M, Alkhouri N. Challenges and opportunities in NASH drug development. Nat Med. 2023;29:562–73.

34. Kong X, Feng D, Wang H, Hong F, Bertola A, Wang FS, et al. Interleukin-22 induces hepatic stellate cell senescence and restricts liver fibrosis in mice. Hepatology. 2012;56:1150–9.

35. Sajiir H, Keshvari S, Wong KY, Borg DJ, Steyn FJ, Fercher C, et al. Liver and pancreatic-targeted interleukin-22 as a therapeutic for metabolic dysfunction-associated steatohepatitis. Nat Commun. 2024;15:4528.

36. Tang KY, Lickliter J, Huang ZH, Xian ZS, Chen HY, Huang C, et al. Safety, pharmacokinetics, and biomarkers of F-652, a recombinant human interleukin-22 dimer, in healthy subjects. Cell Mol Immunol. 2019;16:473–82.

37. Arab JP, Sehrawat TS, Simonetto DA, Verma VK, Feng D, Tang T, et al. An open-label, dose-escalation study to assess the safety and efficacy of IL-22 agonist F-652 in patients with alcohol-associated hepatitis. Hepatology. 2020;72:441–53.